A novel mechanical attachment for biaxial tensile test: Application to formability evaluation for DP590 at different temperatures

Zhihao Wang, Xingrong Chu, Zhenming Yue, Lionel Leotoing, Hong-Jun Gao

Journal of Materials Research and Technology 28 (2024) 4025–4039

Contents lists available at ScienceDirect

Journal of Materials Research and Technology

journal homepage: www.elsevier.com/locate/jmrt

A novel mechanical attachment for biaxial tensile test: Application to formability evaluation for DP590 at different temperatures

Zhihao Wang [a,b], Xingrong Chu [a,*], Zhenming Yue [a], Lionel Leotoing [b], Jun Gao [a]

[a] School of Mechanical, Electrical and Information Engineering, Shandong University, Weihai, 264209, China
[b] Univ Rennes, INSA Rennes, LGCGM (Laboratoire de Génie Civil et Génie Mécanique), F-35000, Rennes, France

ARTICLE INFO

Keywords:
Biaxial tensile test
Nakazima test
Elevated temperatures
Formability
Forming limit curve

ABSTRACT

A novel mechanical attachment for conducting in-plane biaxial tensile test is provided in this paper. In this attachment, the conversion of force from an external actuator into two pairs of orthogonal forces is achieved by specially designed trapezoidal blocks. By using trapezoidal blocks with different inclination angles, biaxial tensile tests of six different tensile ratios can be performed. A heating device is designed for the attachment to conduct thermal biaxial tensile tests. The heating device adopts a combination of the induction heating technology and the conduction heating method. With the developed mechanical attachment and the heating device, the forming limit curves (FLC) of DP590 sheets at ambient temperature, 300 °C, 400 °C and 500 °C are determined using biaxial tensile tests. A classical Nakazima test procedure at ambient temperature is carried out to establish a reference FLC for the material, and the reference FLC is further used to evaluate the results from biaxial tensile tests. Furthermore, an anisotropic GTN model based on Yld2000-3d yield criterion is calibrated by inverse identification procedures and applied to predict the localized necking and fracture for DP590 sheets under biaxial tensions.

1. Introduction

Lightweighting is an increasingly major topic in automotive manufacturing, especially in light of the demands for improving safety and performance while considering energy conservation and emissions reduction. In the design of automotive components, structural optimization is generally combined with the use of lightweight materials towards better weight reduction [1]. The lightweight metallic materials used mainly include advanced high-strength steels and aluminum alloys, etc [2]. These materials provide high strength to weight ratio, corrosion resistance and recyclability, but exhibit high springback and low formability at ambient temperature, which poses a challenge for application in the fabrication of complex shaped components [3]. To overcome this issue, some advanced hot forming techniques have been developed, such as hot stamping for high-strength steels [4], heat treatment forming and in-die quench (HFQ) for aluminum alloys [5]. During hot forming processes, alloys could exhibit complex metallurgical phenomena such as dynamic recovery [6], dynamic recrystallization [7], and dynamic strain aging [8]. These phenomena could cause undesirable microstructural changes and post-form strength deterioration [9], as well as component thickness over-thinning and non-uniform distribution [4]. A profound understanding of mechanical properties of metal sheets over a wide temperature range is necessary for excavating forming potential of the lightweight materials and improving of forming technologies.

The biaxial tensile test is an interesting test method that can characterize mechanical responses of metal sheets under complex loadings and has been increasingly developed and applied in recent years [10]. It has been applied for characterizing various mechanical properties with specimens of different designs: identification of constitutive models [11], characterization of anisotropy behaviors [12], as well as determination of forming limits at necking [13] or fracture [14]. It is worth mentioning that the biaxial tensile test shows significant advantages in the sheet metal formability determination compared to the conventional methods (Nakazima and Marciniak tests). For the conventional methods, a good lubrication between the punch and the specimen is necessary. However, the instability or even failure of the lubrication system due to high temperatures could introduce uncertainty into the formability characterization. The biaxial tensile test works by non-contact stretching of the specimen, eliminating the effects of friction and bending factors, and arbitrary strain paths could be implemented by adjusting the tensile ratio of the two loading axes [15]. However, the biaxial tensile test requires a dedicated testing device, which is expensive and

* Corresponding author.
E-mail address: xrchu@sdu.edu.cn (X. Chu).

https://doi.org/10.1016/j.jmrt.2024.01.023
Received 16 October 2023; Received in revised form 1 January 2024; Accepted 3 January 2024
Available online 8 January 2024

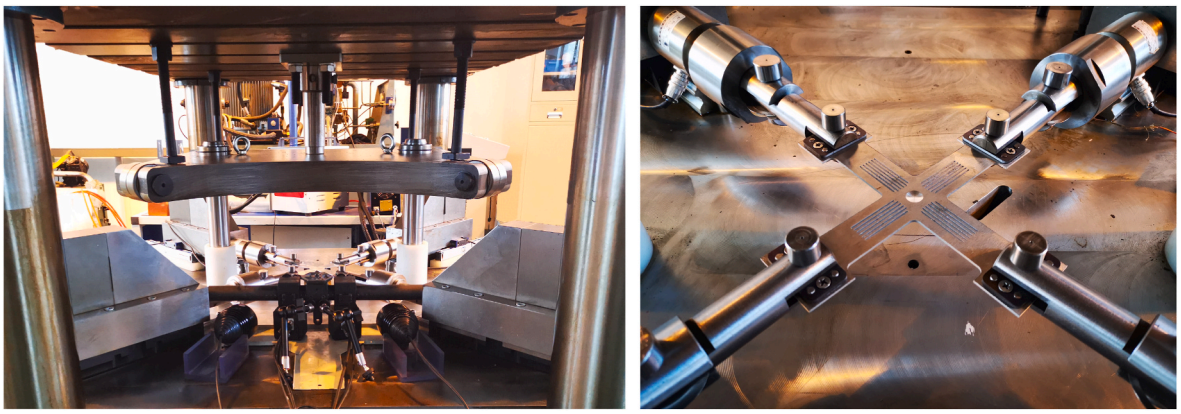

Fig. 1. The mechanical attachment for in-plane biaxial tensile test.

technically complex, limiting its application. Therefore, in this work, as a main objective, a more practical testing device for performing biaxial tensile test is developed.

Preventing the offset of the intersection of the two tensile axes during the biaxial tensile test and allowing adjustable tensile ratios are two main issues in the design of biaxial testing device. In the past few decades, several biaxial testing devices have been developed and can be classified into two groups (ISO 16842, 2014): stand-alone machines and mechanical attachments. The stand-alone biaxial testing machines are generally developed based on independent actuators, such as hydraulics or motors, and use a closed-loop control system to achieve the adjustment of the loading ratios. For instance, Kuwabara et al. [16] developed a biaxial testing apparatus with two pairs of servo-controlled opposing hydraulic cylinders. Symmetrical displacement of opposing hydraulic actuators was ensured through an additional pantograph link mechanism. Leotoing and Guines [17] developed a biaxial testing machine with a horizontal frame and four orthogonally arranged independent servo-hydraulic actuators, which can perform arbitrary proportional quasi-static or dynamic biaxial tensile tests. Chen et al. [18] used four electric cylinders as the power unit in conjunction with a screw transmission structure to construct the biaxial testing machine. A real-time multi-axis motion control algorithm was introduced, ensuring that the center of the specimen remains stationary. The functionality and stability of a stand-alone biaxial testing machine is attractive, but this also leads to high costs and a complex control system.

Mechanical attachment for biaxial loading is an economic alternative. It is developed based on an external actuator (usually a hydraulic machine or a uniaxial tensile tester) and works by converting the external force from the actuator into two pairs of orthogonal forces applied to the specimen. Link mechanisms are often adopted for the force conversion in some existing mechanical attachments. Tierriault et al. [19] presented a complex structure with eight links to realize the equi-biaxial tension on a Ti–Ni cruciform specimen. Recently, a simplified design using four links was proposed and used for equi-biaxial tension [20]. The simplified four-link design sacrifices a certain degree of loading capacity but is more suitable for applications in the field of composite materials and polymer testing. In addition, several apparatuses with specifically designed link structures have been proposed for biaxial testing at different tensile ratios. Bhatnagar et al. [21] designed an apparatus to perform biaxial testing of polymers at four different tensile ratios. The apparatus consists of eight links and two fixed plates. The adjustment of the tensile ratios is achieved by installing links to different positions on the fixed plates. Merklein and Biasutti [22] developed an apparatus with a single out-of-plane screw-driven actuator, adjusting the tensile ratio by modifying the transmission angles of a link mechanism. Shao et al. [23] provided a dedicated mechanical attachment adapted to the Gleeble 3800 tester and performed biaxial tensile tests on aluminum alloy cruciform specimens at three different tensile ratios. This attachment, employing a combination of links and rotatable plates, achieves the adjustment of tensile ratios by replacing links with different lengths. In these apparatuses, the strategy to achieve non-equibiaxial tension involves using different transmission angles for the links of the two pairs of tensile axes. This relies on a complex design comprising multiple links. However, the more links in the apparatus leads to a corresponding decrease in its reliability and loading capacity. In this work, a novel mechanical attachment for biaxial testing with the following advantages is proposed: (1) Ability to perform six different biaxial tensile ratios; (2) High rigidity and stability, meeting the demands of testing high-strength alloy materials; (3) User-friendly design ensures easy installation and simplifies the test setup process. The new mechanical attachment achieves the conversion of the external force into biaxial forces by means of trapezoidal blocks with specially designed inclination angles, offering higher rigidity and loading capacity compared to link mechanisms. The trapezoidal block design and replacement mechanism provides a flexible and efficient solution for biaxial tests at different tensile ratios.

The mechanical properties of various types of lightweight metallic materials under warm or hot forming conditions require continuous research efforts. Plastic models have been proposed to capture the anisotropy [24] and plastic flow [25] behaviors of materials over a wide range of temperatures. In addition, the effect of temperature on the sheet metal formability has been extensively studied, including macroscopic experimental characterization [26] and discussion of the underlying physical processes in hot forming from the microscopic level [27]. Metal sheets are usually subjected to multi-axial loading in actual hot forming, so conducting thermal biaxial tensile tests is essential to validate plastic models and gain a more thorough understanding of the material formability. Several approaches have been developed to achieve thermal test conditions for biaxial tensile test. Liang et al. [28] realized the thermal test conditions for cruciform specimens from ambient temperature to 160 °C by coupling an insulated box fed by a hot air generator with a biaxial tensile machine. Shao et al. [23] used a Gleeble tester equipped with a dedicated mechanical attachment to conduct thermal biaxial tensile tests on AA6082 sheets for formability characterization. The temperature of the specimens was controlled by direct resistance heating and air cooling. The resistance heating approach allows rapid heating of the specimen, but the uniformity of temperature distribution is significantly influenced by the geometry of the specimen. With the similar approach, Zhang et al. [29] characterized the formability of boron steel from 750 to 925 °C under biaxial tensions. Xiao et al. [30] assembled a heating furnace to a biaxial tensile machine, which can realize the thermal test conditions from ambient temperature to 800 °C. The heating furnace was set an observation window to measure the specimen deformation through the digital image correlation (DIC) system. However, the heating furnace is not suitable for mechanical attachments, since the space required for its assembly is limited by the

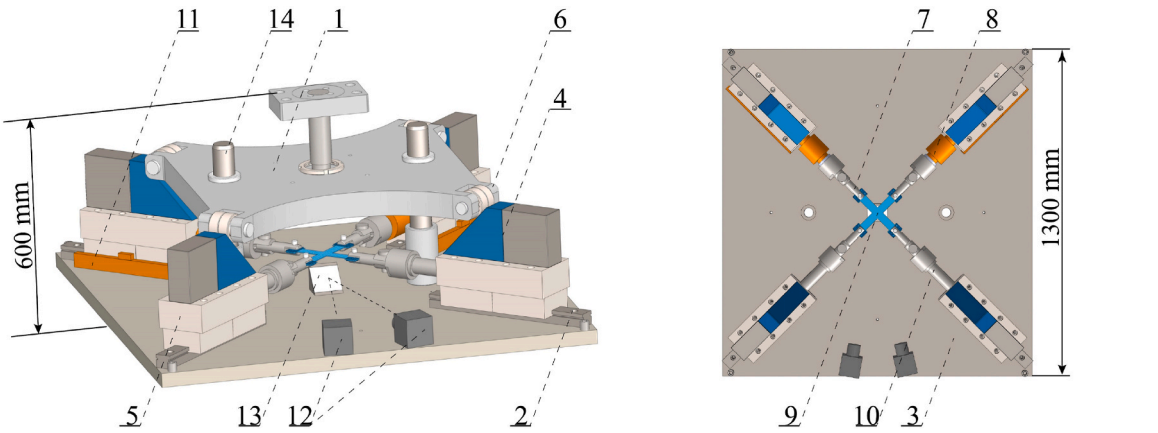

Fig. 2. Schematic diagram of the mechanical attachment.

force-transferring structures. Therefore, the need to develop an appropriate heating device for the mechanical attachment is evident. The heating device has to be devised the following characteristics: (1) Ability to provide a wide test temperature range; (2) Allowing for uniform temperature distribution in specimens; (3) Good adaptability to various materials and specimen geometries.

In the following sections, a novel mechanical attachment for in-plane biaxial tensile test and a heating device are presented. The mechanical attachment has a simple and reliable mechanical structure, and allows to perform biaxial tensile tests of six different tensile ratios. The heating device combines the induction heating technique and conduction heating method to provide faster heating rate and higher temperatures while allowing for uniform temperature distribution within the main heating zone of specimen. To validate the proposed mechanical attachment and heating device, the determination of FLCs for DP590 sheets at ambient temperature, 300 °C, 400 °C and 500 °C are performed. A classical Nakazima test procedure is also conducted to establish a reference FLC for the material at ambient temperature, and the reference FLC is further used to evaluate the results from biaxial tensile tests. Furthermore, the Yld2000-3d yield criterion for DP590 sheets at ambient temperature is calibrated by inverse analyses with an equi-biaxial tensile test. Then, a GTN damage model coupled with Yld2000-3d yield criterion is employed to predict the localized necking and fracture of DP590 sheets under biaxial tensions.

2. Novel mechanical attachment for in-plane biaxial tension

In Fig. 1, the novel mechanical attachment designed for conducting biaxial tensile tests is presented, which has been integrated into a servo-hydraulic press machine. The attachment has four orthogonally arranged trapezoidal blocks with designed inclination angles, which can convert the vertical force generated by the press machine into four horizontal forces exerted on the cruciform specimen. This design allows the change of trapezoidal blocks with different inclination angles to perform biaxial tensile tests with different tension ratios.

Fig. 2 illustrates the schematic diagram of the mechanical attachment. The upper plate (1) is bolted to the cross beam of the press machine, and four support columns are used to enhance the structural rigidity of the upper plate, preventing it from tilting and bending under loading. Four linear guides (2) are symmetrically fixed on the bottom plate (3) along two tensile axes. Two pairs of trapezoidal blocks (4) with the bases (5) are assembled on the linear guides. As the upper plate moved in a downward direction, the cylinder roller bearings (6) installed at the corners of the upper plate actuate the trapezoidal blocks to move simultaneously along the linear guides. For each pair of bases, two specimen fixtures (7) are connected on the one side through a pull rod (8) and on the other side through a force sensor (9). Thus, the load from the trapezoidal block can be transmitted to the cruciform specimen (10) via the fixture and measured by the force sensor. In addition, the displacement of the trapezoidal block is measured by a grating ruler displacement sensor (11), which is equipped on the side of the base. The cruciform specimen is clamped horizontally at the center of the mechanical attachment. Vertical movement of the specimen is restricted, but rotation in the horizontal plane is permitted.

A DIC system (12) with two high resolution cameras is employed to measure strain fields of specimens during the test. For the convenience of capturing the DIC-images, an optical flat mirror (13) is placed below the specimen at 45°. The length and width of the mechanical attachment are 1300 mm, and the height is 600 mm. According to the verification of structural rigidity by numerical simulations, for each tensile axis, the maximum load capacity is 100 kN, and the maximum displacement is 100 mm. The test velocity can be directly controlled by the servo-hydraulic press machine ranging from 0.05 mm/min to 200 mm/min. The developed mechanical attachment is adapted to test cruciform specimens with a length of 230 mm.

The trapezoidal block is the core component of this attachment as it

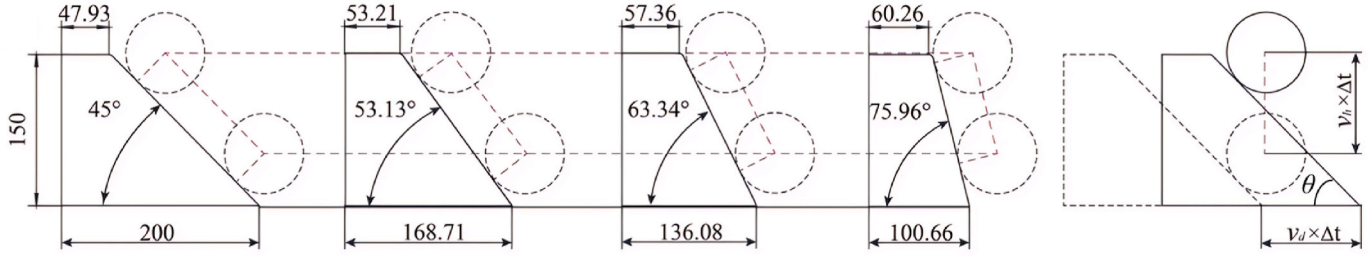

Fig. 3. Dimensions of trapezoidal blocks with different inclination angles θ.

Table 1
Combinations of trapezoidal blocks with different inclination angles θ and the corresponding biaxial tensile ratios k.

θ_x of X-axis	θ_y of Y-axis	tan θ_x	tan θ_y	Tensile ratio k
45°	45°	1	1	4 : 4
45°	53.13°	1	1.333	4 : 3
45°	63.34°	1	2	4 : 2
45°	75.96°	1	4	4 : 1
53.13°	63.34°	1.333	2	3 : 2
53.13°	75.96°	1.333	4	3 : 1

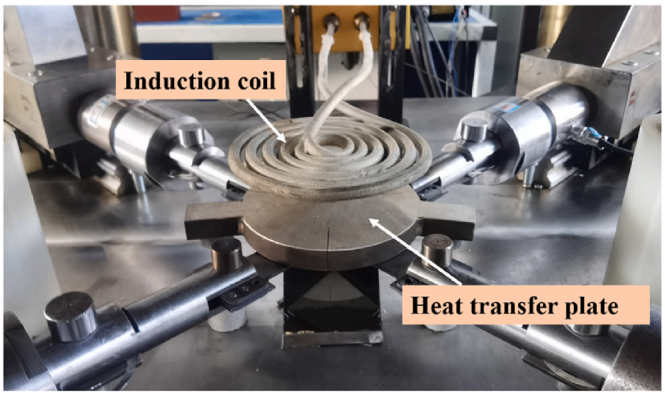

Fig. 4. Heating system for thermal biaxial tensile test.

determines the biaxial tensile ratio. As shown in Fig. 3, with different inclination angles θ, the trapezoidal block allows for the conversion of vertical displacement into different horizontal displacements. In this work, six biaxial tensile ratios between the two tensile directions (X and Y axes) are realized through adjusting the combination of trapezoidal blocks with different θ angles, as presented in Table 1. And the biaxial tensile ratio k is calculated from the θ,

$$k = \frac{v_{d,x\text{-}axis}}{v_{d,y\text{-}axis}} = \frac{v_h/\tan\theta_x}{v_h/\tan\theta_y} = \frac{\tan\theta_y}{\tan\theta_x} \tag{1}$$

A heating device is designed for the mechanical attachment for performing thermal biaxial tensile tests. The heating device uses a combination of the induction heating technology and the conduction heating method which allows the heating of cruciform specimen up to 700 °C. As shown in Fig. 4, a heat transfer plate is placed above the specimen in parallel with a small gap and heated by a high-frequency induction heating device through an induction coil. The plate is made of Inconel 718 alloy and is supported by three height-adjustable support columns. At the same time, the cruciform specimen is heated by heat conduction and radiation from the hot plate. A K-type thermocouple wire is attached to the specimen central area for temperature monitoring, and the measured temperatures are used in the feedback control of the induction heating device through a programmable logic controller (PLC). In addition, to avoid overheating of the heat transfer plate, the temperature of the plate is also monitored by a thermocouple wire and limited by the PLC. Compared with the traditional resistance-wire heating or furnace heating methods, the proposed heating approach allows faster heating rates and higher temperatures to be reached. Furthermore, the use of the heat transfer plate avoids the non-uniform distribution of specimen temperature caused by the non-uniform magnetic field of the induction coil and the skin effect [31] of high-frequency induction heating, which also makes the heating device applicable to metallic and nonmetallic specimens.

3. Determination of FLCs for DP590 using biaxial tensile tests

In this section, the FLCs of DP590 sheets at ambient temperature, 300 °C, 400 °C and 500 °C are determined using the mechanical attachment and the heating device. The cruciform specimen [32] depicted in Fig. 5 is adopted for biaxial tensile tests. The specimen has a reduced thickness at the center region to induce the necking and initial crack near the specimen center. The cruciform specimens are obtained from a 2 mm thick DP590 sheet using laser cutting. The thickness reduction is performed by CNC machining. The DIC system is employed to measure the strain fields. Since all tests are performed at quasi-static strain rates, a DIC-images acquisition frequency of 12 images/sec is adopted. Strain fields are calculated using a subset of 14 × 14 pixels^2 and step distance of 7 pixels.

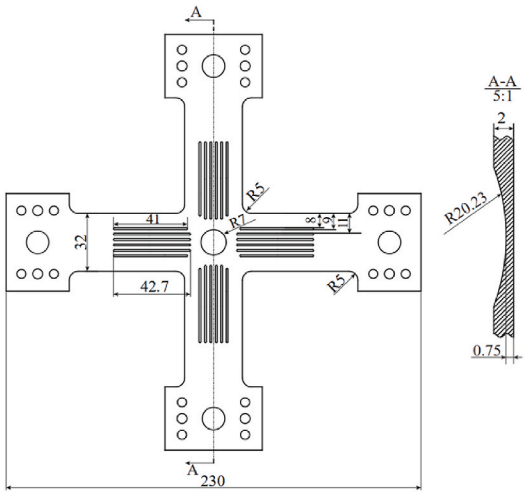

Fig. 5. Dimensions of the cruciform specimen for FLC determination (unit: mm).

3.1. Biaxial tensile tests at the ambient temperature

Biaxial tensile tests at the ambient temperature are conducted for five different tensile ratios (4 : 4, 4 : 3, 3 : 2, 4 : 2, and 4 : 1) to evaluate forming limits at necking under different strain paths. The downward velocity of the cross beam of the press machine is set to 4 mm/min. Each tensile ratio is performed twice to ensure the repeatability of results. The central region (32 × 32 mm^2) of the specimen non-thinned side is selected as the region of interest (ROI) for strain measurement.

Fig. 6 (a) shows the strain paths up to fracture extracted from the center of the ROI. The obtained strain paths cover the range from plane strain to equi-biaxial stretching and are approximately linear until localized necking occurs. In a recent study [13], the ISO method (ISO 12004-2, 2008) was recommended for the cruciform specimens with thickness reduction to determine forming limit curves. Consequently, in the present work, forming limit points are determined using the ISO method and plotted as circular symbols in Fig. 6 (a). The ISO method works by an inverse parabolic fitting to the major strain distribution, as illustrated in Fig. 6 (b). The major strains are extracted from a single path perpendicular to the localized necking zone and passing through the specimen center. The fitting windows on the both sides of the crack are defined based on the second derivative of the major strain. The major limit strain is determined by the vertex of the fitted parabola, and the minor limit strain is obtained from the strain pair of the measured strain path according to the major limit strain. The major limit strains for DP590 sheets show an increase from plane strain to equi-biaxial tension, while the fracture strains gradually decrease. Since the adopted cruciform specimen is intended for characterizing the formability of metal sheets in the first quadrant, the obtained strain paths do not involve the range from plane strain to uniaxial tension. Thus, tensile test using dog-bone specimen is performed to obtain the forming limit point at the uniaxial tension state. The dimensions of the dog-bone specimen can be

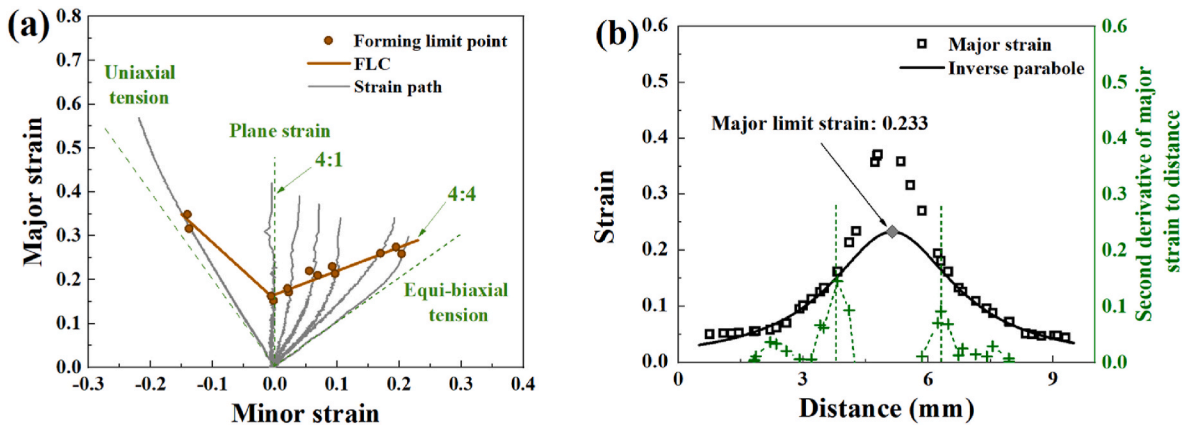

Fig. 6. (a) Forming limit points with corresponding strain paths and FLC for DP590 sheets at ambient temperature. (b) Major limit strain measurement using the ISO method.

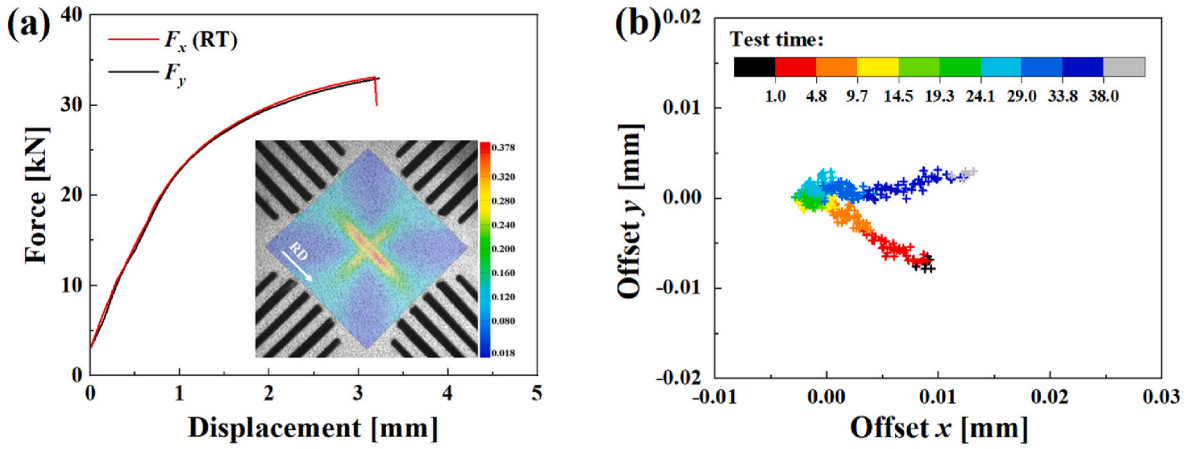

Fig. 7. Experimental results for the 4:4 biaxial tensile test (equi-biaxial tension): (a) force vs. displacement curves for both tensile axes along with the major strain field of the specimen interested area; (b) Offsets of the specimen center point, with different colored symbols indicating the offset of different test times.

found in Fig. 19 (a). The determination of forming limit for uniaxial tension is also based on the ISO method. The major strains are extracted from the DIC image just before the crack occur, and the path for major strain extraction is perpendicular to the localized necking zone. The FLC of DP590 sheets at ambient temperature is established by connecting forming limit points with two smooth curves.

The developed mechanical attachment is well capable of performing biaxial tensile tests with different tensile ratios. In particular, the strain path along the ideal equi-biaxial tension state is observed in the 4 : 4 biaxial tensile test (equi-biaxial tension), indicating that the expected

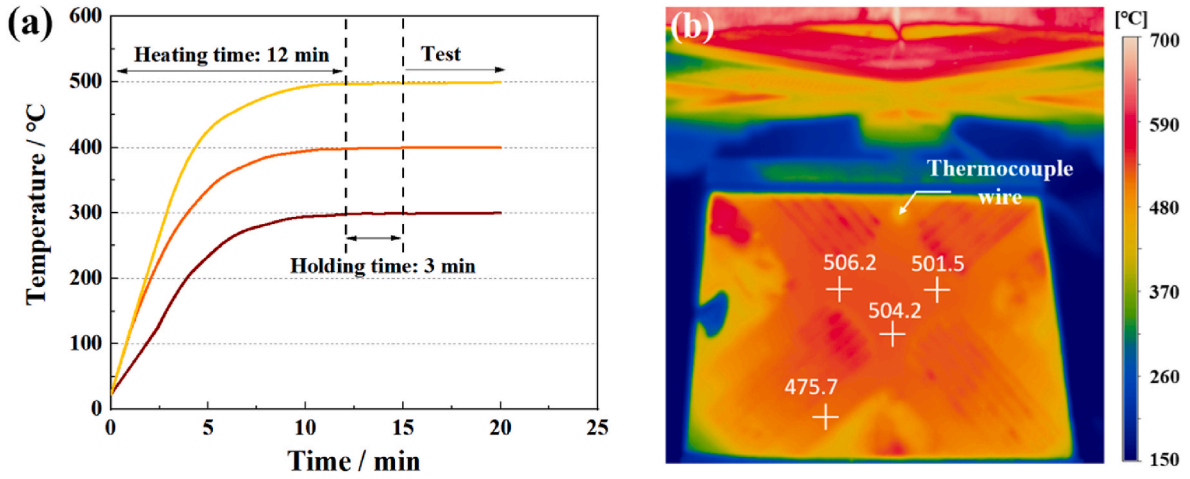

Fig. 8. (a) Measured temperature histories of the specimen central area for target test temperatures of 300 °C, 400 °C and 500 °C. (b) Temperature distribution of the specimen at the target test temperature of 500 °C.

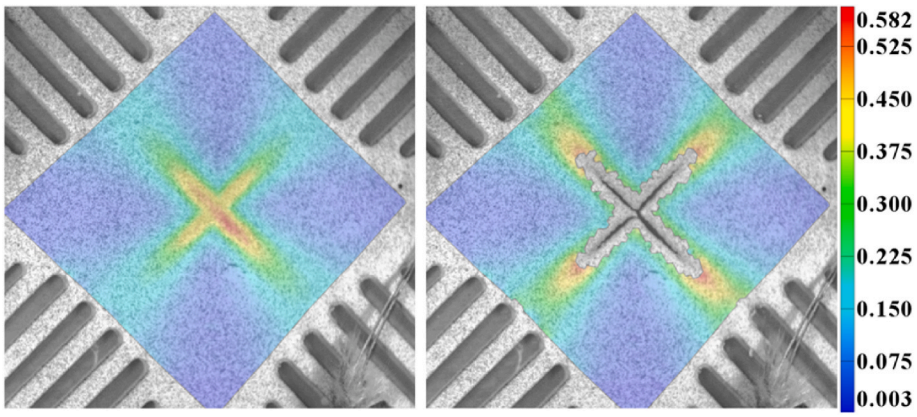

Fig. 9. Major strain field (at the test time of 24 s) and cracks of the cruciform specimen tested under equi-biaxial tension at 500 °C.

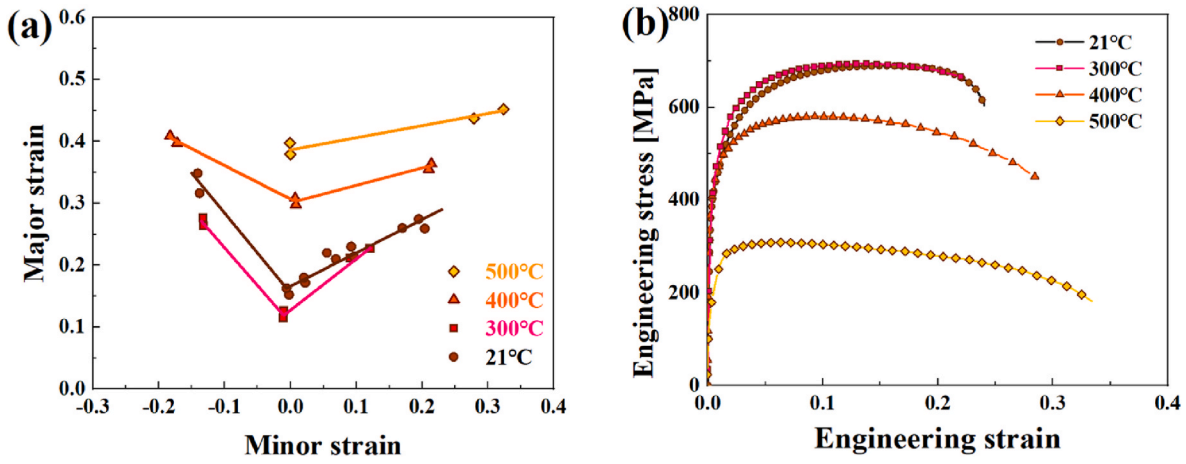

Fig. 10. (a) FLCs of DP590 sheets at different temperatures determined using biaxial tensile tests. (b) Engineering stress vs. strain curves of DP590 sheets from uniaxial tensile tests at different temperatures.

simultaneous loading of the two tensile axes is achieved. Fig. 7 (a) presents the force vs. displacement curves for both tensile axes obtained from the 4 : 4 biaxial tensile test, along with the major strain field of the ROI before the onset of crack. During the test, F_x and F_y are remain in good agreement, where F_x is the tensile force measured along the specimen rolling direction (RD). This results in a cross-shaped major strain distribution on the cruciform specimen. The offset of the specimen center point during the test is plotted in Fig. 7 (b), with different colored symbols indicating the measured offset corresponding to different test times. At the beginning of tension, the specimen is automatically positioned to the center of the mechanical attachment by biaxial forces. Then, the specimen center point remains stable during the test, with slight offsets. After necking occurs, the specimen center point shifts along the positive *x*-axis (corresponding to the material rolling direction). The above results demonstrate the good performance of the developed mechanical attachment.

3.2. Biaxial tensile tests at the elevated temperatures

Determination of thermal FLCs for DP590 sheets is carried out at 300 °C, 400 °C and 500 °C. Tests at higher temperatures are not performed because the spray paints used for speckle pattern fail at temperatures above 500 °C. Three representative strain paths are considered for the thermal FLCs determination: plane strain, equi-biaxial and uniaxial tensions. The equi-biaxial tension and plane strain states are provided by 4 : 4 and 4 : 1 biaxial tensile tests, respectively. Each test condition is preformed twice to ensure the repeatability of results. A thermocouple wire for temperature controlling is welded at the boundary of the specimen central area. As shown in Fig. 8 (a), the specimen is heated to the target temperature for about 12 min and held at the target temperature for 3 min before starting the test. During the test, the temperature control error of the specimen is less than 6 °C. Fig. 8(b) illustrates the temperature distribution of the specimen at the target test temperature of 500 °C, measured using an infrared camera (Optris Xi400). The infrared camera has been calibrated based on thermocouple measurements. The temperature is uniformly distributed within the specimen ROI and gradually decreases at the arms. The major strain field (from the DIC image just before crack initiation) and cracks of the cruciform specimen from the 4 : 4 tensile test at 500 °C are shown in Fig. 9. The major strain distribution and cracks are cross-shaped. This demonstrates the symmetry of the specimen temperature distribution and the simultaneous loading of the two tensile axes at elevated temperatures.

Fig. 10 (a) shows the FLCs of DP590 sheets at different temperatures. The thermal FLC is constructed by connecting the forming limit points with two straight lines. This is in light of that the obtained forming limit points of DP590 sheet at ambient temperature can be approximately fitted by two straight lines. Due to the failure of the spray paint caused by excessive deformation of the specimen stretched under the uniaxial tension state at 500 °C, the limit strains at necking are not obtained. The FLCs reveal that the formability of DP590 sheets has a non-monotonic dependence on the forming temperature. The formability is significantly improved at 400 °C and 500 °C compared to the ambient temperature. However, the FLC at 300 °C is close to that at ambient

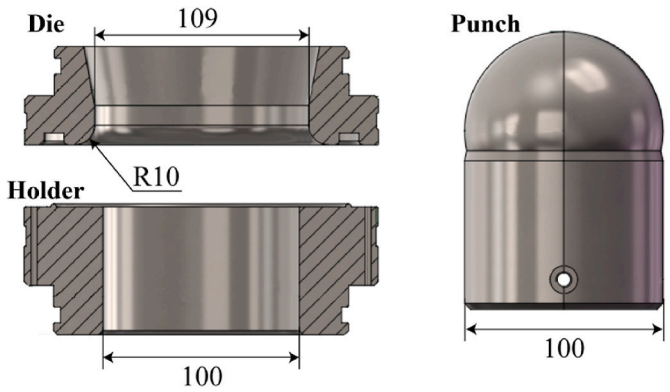

Fig. 11. Schematic diagram of the toolset for the Nakazima tests (unit: mm).

temperature and even lower under the plane strain and uniaxial tension strain states. This can be attributed to the dynamic strain aging effect (DSA) [33]. The lower formability for DP590 at 300 °C was also reported by Simsir et al. [34]. Fig. 10 (b) shows the engineering stress vs. strain curves of DP590 sheets obtained from uniaxial tensile tests at different temperatures. The gauge size of the uniaxial tension specimen is 50 × 12 mm^2. It is found that the strength of DP590 sheets at 300 °C is higher than that at 21 °C. The increase of strength at elevated temperatures is a typical manifestation of the DSA effect [35]. The work of Bayramin et al. [36] reported that the effects of DSA on DP590 are most intense at 300 °C.

4. Nakazima tests at ambient temperature

The Nakazima test, as recommended by ISO 12004-2, is a classical approach to determine the forming limit strains at necking. In this section, the Nakazima test is carried out to obtain a reference FLC of material at ambient temperature, and the result is further used to assess the FLC determined by the biaxial tensile tests. The toolsets of the Nakazima test are schematically depicted in Fig. 11. A punch with a radius of 50 mm is used. The die takes an inner radius of 54.5 mm with an entry radius of 10 mm. The specimen dimensions are given in Fig. 12 (a), in which R represents the notch radius. To generate various strain paths from uniaxial tension to equi-biaxial tension, seven different values of R are employed: 0, 20, 40, 50, 60, 70, and 80 mm. The specimens are formed at a test velocity of 0.016 mm/s until fracture, and each specimen geometry is tested three times to ensure the repeatability. To induce the initial crack near the specimen center, the lubrication measure of grease-permeated cotton and silicone composite sheet is used between the specimen and the punch. Fig. 12 (b) shows the specimens with fracture.

Fig. 13 (a) shows the forming limit points obtained from the Nakazima tests along with their corresponding strain paths. The specimen with $R = 0$ (corresponding to a circular specimen) generates a linear strain path, following the equi-biaxial tension state until fracture. While, the strain paths of other specimens are non-linear with a significant biaxial pre-strain at the initial test stage. This biaxial pre-strain can be attributed to the bending of the specimen caused by the hemispherical punch. The forming limit strains are determined using the ISO method as per ISO 12004-2. Major strains along three cross-sections perpendicular to the localized necking zone are extracted for the inverse-parabola fitting. The mean value of the three fitting results is adopted as the major limit strain. The FLC is then obtained by connecting the forming limit points with two smooth lines.

A comparison between the FLCs determined from the biaxial tensile tests and the Nakazima tests is presented in Fig. 13 (b). It can be seen

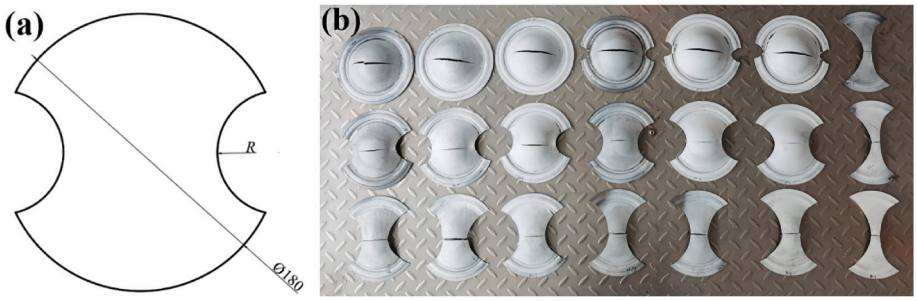

Fig. 12. (a) Dimensions of the Nakazima test specimen (unit: mm), and (b) photographs of specimens with fracture.

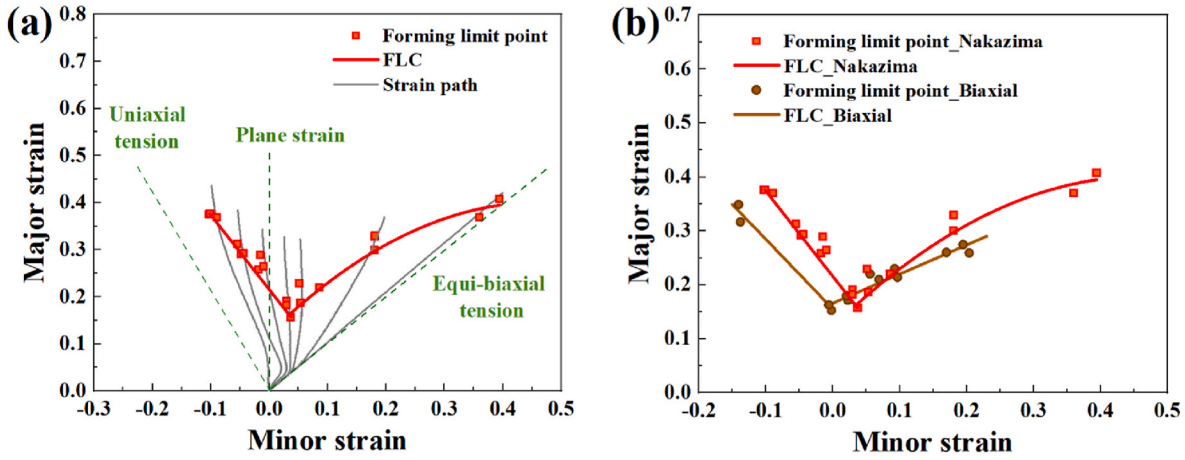

Fig. 13. (a) Forming limit points with corresponding strain paths and FLC for DP590 sheets determined by the Nakazima tests. (b) Comparison between the FLCs determined by the Nakazima tests and the biaxial tensile tests.

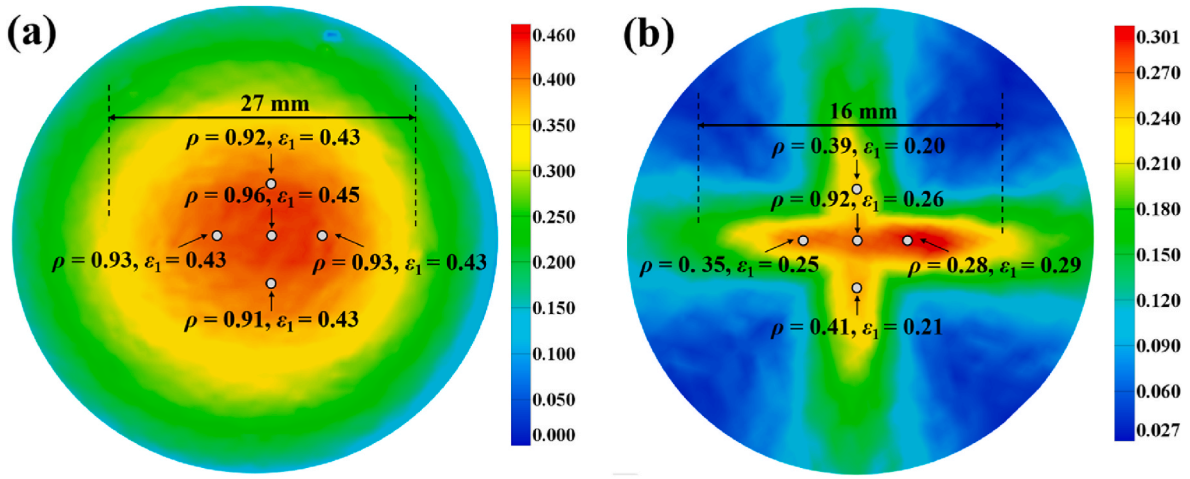

Fig. 14. Major strain fields and principal strain ratios of main deformation regions from (a) the Nakazima test using the specimen with $R = 0$ and (b) the 4 : 4 biaxial tensile test. The strain fields correspond to the moments of localized necking occurs.

that the FLC obtained by the Nakazima tests has an offset towards the positive value of minor strain of about 0.04 strain. This offset is caused by the strain path nonlinearity of the Nakazima tests. For the FLC obtained by the biaxial tensile tests, the minor strain at the FLC_0 (the lowest point) is −0.006 thanks to the in-plane forming and frictionless process conditions. The major limit strains of FLC_0 determined by the two test approaches are approximately the same. The FLC_0 of the Nakazima test is provided by the specimen with $R = 50$ mm, and the major limit strain of FLC_0 is 0.157. The FLC_0 of the biaxial tensile test is obtained from the tensile ratio of 4 : 1, and the major limit strain of FLC_0 is 0.162. While, for the equi-biaxial tension strain state, the Nakazima test gives a significantly higher estimation of formability than the biaxial tensile tests. In a related study, Zhang et al. [37] conducted a comparison of biaxial tensile tests and Nakazima tests, focusing on the formability of AA5754 sheets. A dedicated cruciform specimen with double-side thickness reduction was developed for biaxial testing. The obtained forming limits under equi-biaxial tension state from biaxial tests were also significantly lower than that from the Nakazima tests. This divergence was attributed to pronounced stress and strain gradients within the ROI of the cruciform specimen. Lionel et al. [15] presented a work comparing the biaxial tensile test and the Marciniak test for determining the FLC of AA5086 sheets. The results showed that the two experimental procedures gave comparable formability estimates for the material, ranging from equi-biaxial tension to plane strain. However, a higher estimate was obtained from the biaxial testing as the sheet deformed under uniaxial tension condition.

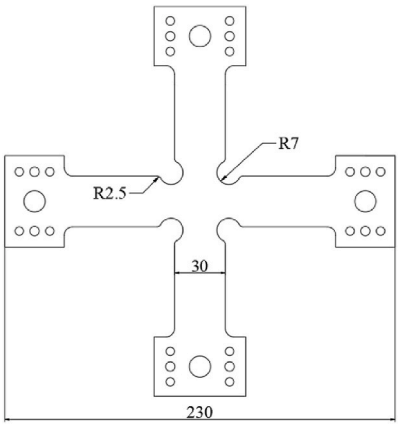

Fig. 15. Dimensions of the cruciform specimen for Yld2000-3d calibration (unit: mm).

Considering the divergence in forming limits at the equi-biaxial state determined by the two experimental procedures in the present work, discussions involving the Nakazima test using a specimen with $R = 0$ and the 4 : 4 biaxial tensile test are as follows. The principal strain ratio ρ is defined as $\rho = \varepsilon_{minor}/\varepsilon_{major}$. As shown in Fig. 14, for the Nakazima test, the strain state within the main deformation region of the specimen with $R = 0$ is uniform and close to the equi-biaxial tension state ($\rho = 1$), ensuring that the localized necking occurs under the equi-biaxial tension state. While, for the biaxial tensile test, the strain state within the main deformation region is non-uniform. Only the center point is close to an equi-biaxial tension state, while the strain state of the nearby region is in an intermediate strain state between equi-biaxial tension and plane strain. The localized necking occurs away from the specimen center. This is because the intermediate strain state between equi-biaxial tension state and plane strain at the necking initiating area reduces the forming limit strain to necking. Although the specimen thickness is reduced to a dome profile, the strain gradient at center area is low, which allows the localized necking to occur first in an off-center region. Therefore, the forming limits of DP590 sheets at the equi-biaxial tension state determined using the adopted cruciform specimen is conservative.

It is worth mentioning that, the same cruciform specimen geometry was employed in the previous works to determine the formability of DP600 [32] and AA6061-T4 [13] sheets by biaxial testing using a servo-hydraulic biaxial tester. For both materials under equi-biaxial tension, localized necking and initial fracture occurred at the center of the cruciform specimen, without encountering deviations from the center as observed in the present work. To address the potential influence of the biaxial test attachment and specimen manufacturing precision factors on the observed off-center necking in this study, numerical biaxial tensile tests are conducted using an anisotropic GTN plasticity model in Section 5.

5. FLC prediction using an anisotropic GTN model

The localized necking, as a precursor to fracture, is influenced by the accumulation of damage during plastic forming processes [38,39]. In this section, the GTN model ([40], given in Appendix. 1) with the Yld2000-3d anisotropy yield criterion ([41], given in Appendix. 2) is selected to predict the localized necking fracture of DP590 sheets in the biaxial tensile tests at ambient temperature. The parameters of the GTN model and the Yld2000-3d yield criterion are identified through two inverse identification procedures, respectively. Both identification procedures are based on the finite element model updating (FEMU) method [42]. The principle of the FEMU is to identify an optimal set of material parameters by optimizing predictions to approximate experiments until

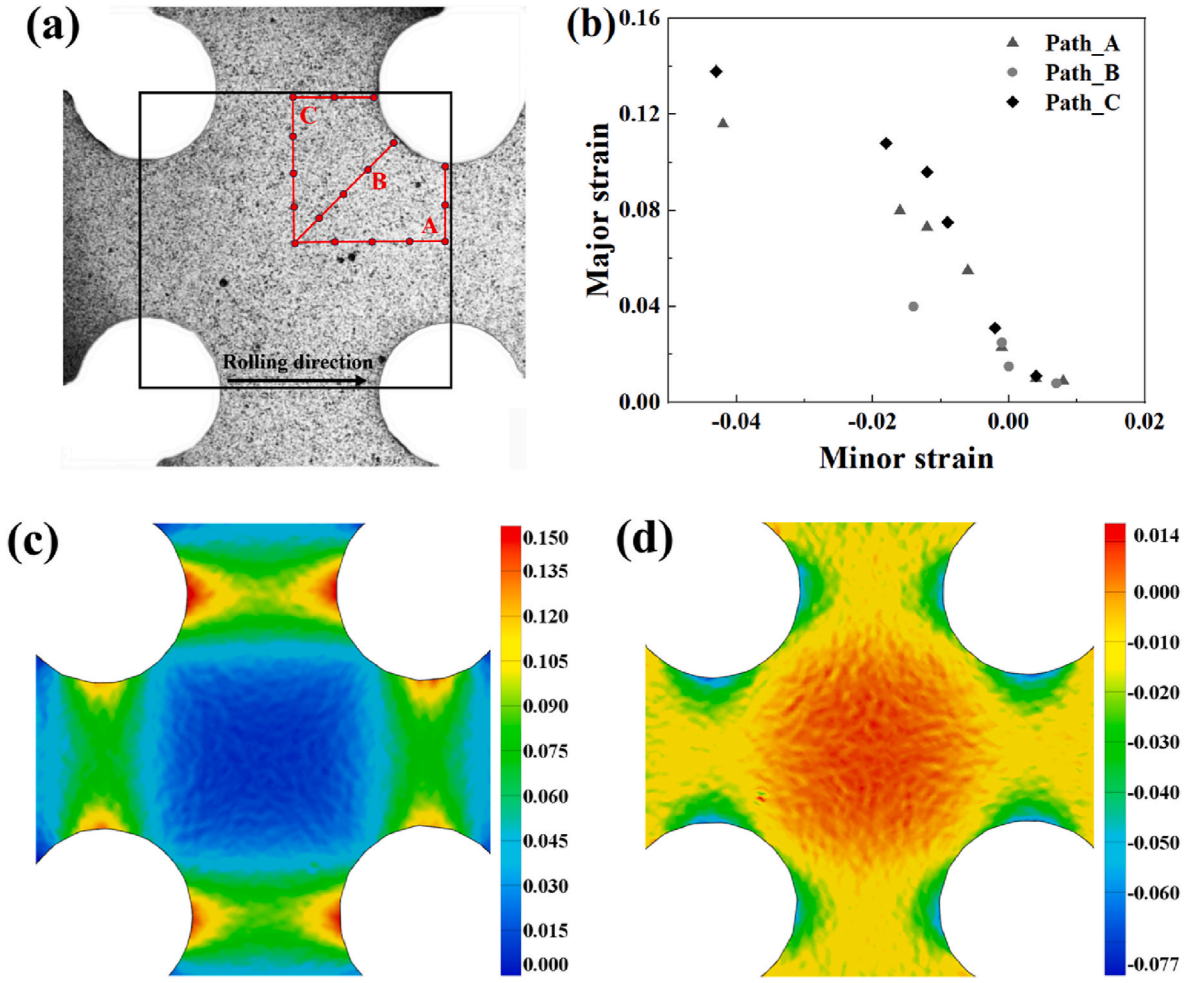

Fig. 16. (a) The selected ROI and material points for extracting major and minor strains. (b) Major and minor strains extracted from the selected material points at the test time of 46 s. (c) Major and (d) minor strain fields of the ROI at the test time of 46 s.

the two match as closely as possible [43]. The constitutive modeling in the present work is only applicable to the formability prediction of DP590 at ambient temperature. Considering the DSA effects exhibited by DP590 sheets, as well as the effect of temperature on anisotropy and damage evolutions, an advanced constitutive modeling is necessary for the temperature-dependent formability prediction, which will be considered in our future work.

5.1. Yld2000-3d calibration using an equi-biaxial tensile test

The experimental measurements for Yld2000-3d parameters calibration are obtained from an equi-biaxial tensile test using the cruciform specimen depicted in Fig. 15. The specimen was proposed by Martins et al. [44], which can generate a heterogeneous strain field to exhibit the anisotropy of the material. As shown in Fig. 16 (a), the specimen central area (34 mm × 34 mm) is selected as the ROI. The measured major and minor strain fields within the ROI at the test time of 46 s are given in Fig. 16 (c) and (d). This test time is before localized necking occurs and the equivalent strain near the specimen notch reaches 0.15. It can be found that the strain state in the ROI exhibits significant heterogeneous. From the specimen center to the boundary area, the strain state transitions from equal-biaxial tension to uniaxial tension. Due to the heterogeneity, various regions of the specimen experience different stress states and strain paths, and thus a wealth of information about material anisotropy can be extracted [45]. Three paths (indicated as red lines) are defined within the ROI, with several material points defined along these paths. These material points cover representative strain states of the ROI, as illustrated in Fig. 16 (b). Subsequently, the major and minor strains extracted from these material points are employed as experimental measurements for the inverse identification procedure.

The numerical predictions are obtained by reproducing the equi-biaxial tensile test with a FE model in the ABAQUS/Standard software. Considering the symmetry, a quarter of the cruciform specimen is modeled. The mesh size is refined to 0.5 mm within the main deformation region of the specimen. The Yld2000-3d yield criterion is implemented through a UMAT subroutine, and the hardening of the material is defined by a modified Voce function (Eq. (2)). Experimentally measured forces of both tensile axes are applied to the cruciform specimen in the FE model. A cost function (Eq. (3)) is used to quantify the gap between the experimental and numerical principal strains. The Yld2000-3d yield criterion contains 12 parameters $\alpha_1 \sim \alpha_{12}$. In this work, only the calibration of the parameters $\alpha_1 \sim \alpha_8$ is considered, while the values of $\alpha_9 \sim \alpha_{12}$ are set to 1 [46]. The recommended value of the exponent $a = 6$ in Yld2000-3d is adopted for DP590 sheets [47].

$$\sigma = \sigma_0 + K \cdot \left[1 - \exp\left(-n \cdot \bar{\varepsilon}_p\right)\right] + H \cdot \varepsilon_p \tag{2}$$

where σ_0 is initial yield stress. K, n, H are material parameters. Based on the true stress vs. plastic strain data of DP590 sheets, the values of the material parameters are determined as: $\sigma_0 = 399.65$ MPa, $K = 277.79$ MPa, $n = 35.43$, and $H = 846.44$ MPa. The true stress vs. plastic strain data is calculated from a uniaxial tensile test of the material RD.

Table 2
The calibrated parameters of Yld2000-3d yield criterion for DP590 sheets.

α_1	α_2	α_3	α_4	α_5	α_6	α_7	α_8
0.959	1.010	0.975	1.016	1.011	0.934	0.957	0.983

$$G(\alpha_1 \sim \alpha_8) = \sum_{i=1}^{p}\left[\sqrt{\left(\frac{\varepsilon_{major}^{exp} - \varepsilon_{major}^{num}}{\overline{\varepsilon}_{major}^{exp}}\right)^2} + \sqrt{\left(\frac{\varepsilon_{minor}^{exp} - \varepsilon_{minor}^{num}}{\overline{\varepsilon}_{minor}^{exp}}\right)^2}\right] \quad (3)$$

where i is an index indicating the material points for principal strain extracting. ε_{major} and ε_{minor} donate the major and minor strains, respectively. ε^{exp} and ε^{num} donate the experimental and numerical strains, respectively.

The inverse identification procedure is carried out on the mode-FRONTIER platform, and the optimization of anisotropy parameters is achieved by coupling the SIMPLEX algorithm with the cost-function. The inverse identification procedure is performed for 1000 iterations and an optimal solution is selected from 7 convergences. Each iteration of the parameter set requires performing a FE job and evaluating the gap with the cost-function, then the SIMPLEX algorithm generates a new parameter set according to the value of the cost-function. Table 2 gives the final identified parameters of Yld2000-3d yield criterion for DP590 sheets. Fig. 17 presents the numerical major and minor strain fields. The predicted major and minor strain fields reach a good agreement with the experimental results in Fig. 16. Fig. 18 (a) plots the r-values and normalized yield stresses predicted by the calibrated Yld2000-3d against the experimental results determined by uniaxial tensile tests. The comparison shows that the calibrated Yld2000-3d parameters using the equi-biaxial tensile test can precisely describe the anisotropy of DP590 sheets.

5.2. GTN model calibration

The adopted GTN model contains 10 parameters: q_1, q_2, q_3, f_0, f_N, f_C, f_F, ε_N, s_N, k_w. In this work, the recommended values of $q_1 = 1.5$, $q_2 = 1$ and $q_3 = 2.25$ are used [48]. The remaining parameters are calibrated by an inverse identification procedure. The experimental program for the inverse identification involves three tests with different stress triaxialities: tensile tests using a dog-bone specimen ($\eta = 0.33$) and a central hole specimen ($\eta = 0.44$), and Nakazima test using the specimen with $R = 0$ ($\eta = 0.66$). The GTN parameters are calibrated by minimizing the gap between the predicted and experimental force-displacement

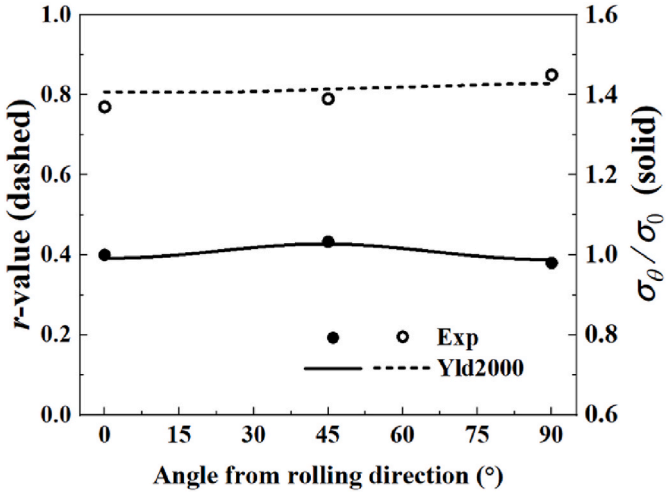

Fig. 18. Experimental and Yld2000-3d predicted r-values and yield stresses.

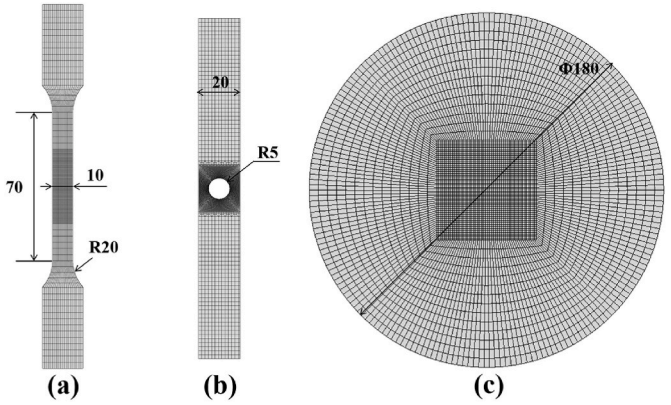

Fig. 19. FE models of the (a) dog-bone specimen, (b) central hole specimen, and Nakazima test specimen with $R = 0$, along with specimen dimensions (unit: mm).

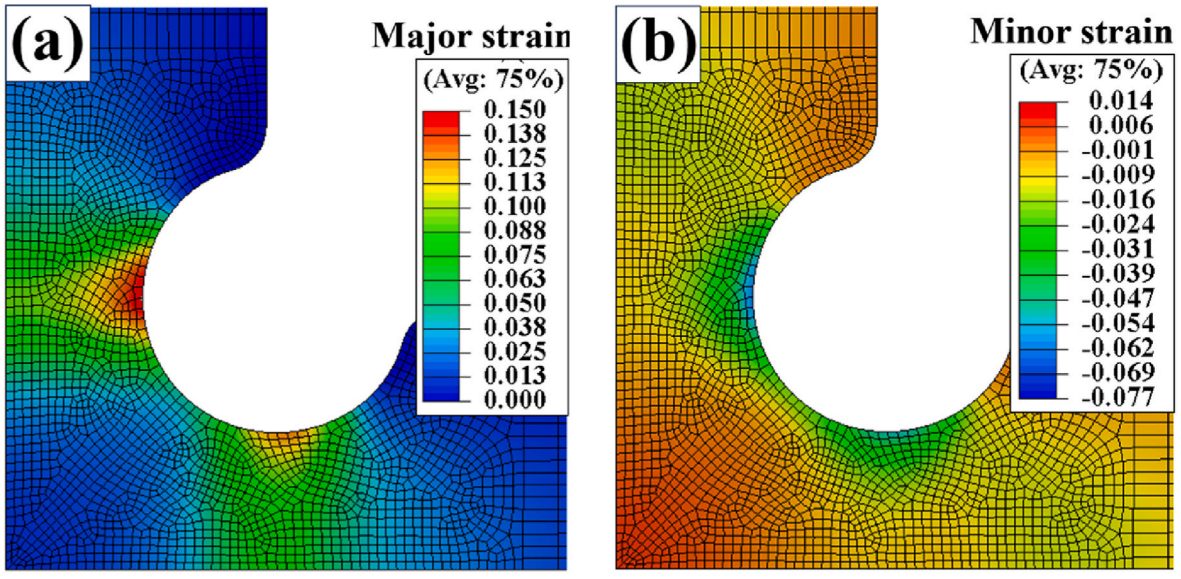

Fig. 17. Predicted (a) major and (b) minor strain fields based on the calibrated Yld2000-3d yield criterion.

Table 3
The calibrated parameters of GTN model for DP590 sheets at ambient temperature.

Parameter	f_0	f_C	f_F	f_N	ε_N	s_N	k_w
Value	0.00005	0.067	0.125	0.02	0.3	0.09	8

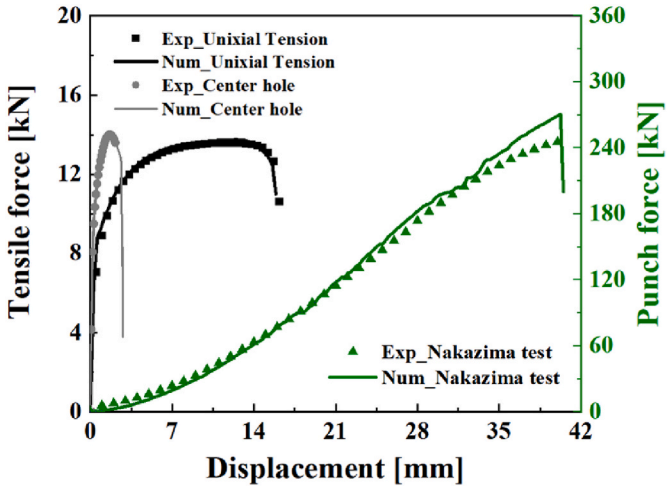

Fig. 20. Comparison of experimentally measured and predicted force-displacement curves.

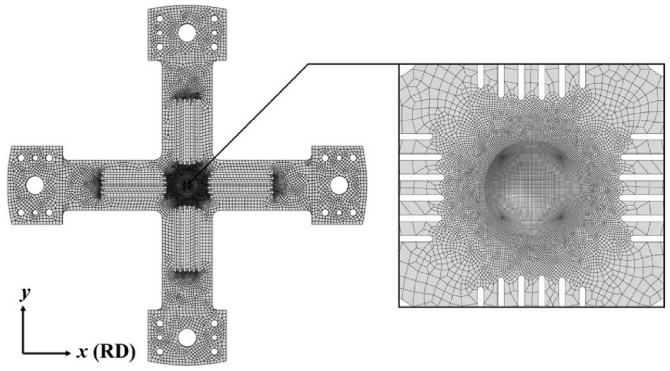

Fig. 21. The FE model of the cruciform specimen for the FLC prediction.

curves of these three tests. Fig. 19 illustrates the used FE models for the three tests along with specimen dimensions and mesh sizes. The FE models are built in the ABAQUS/Explicit software. The user subroutine VUMAT is employed to implement the anisotropic GTN model. The material anisotropy is defined using the calibrated Yld2000-3d in section 5.1. The identified GTN parameters for DP590 sheets are summarized in Table 3. A good agreement between the predicted force-displacement curves and experimentally measured results is achieved, as shown in Fig. 20.

5.3. Numerical biaxial tensile tests

Subsequently, the FE model of the cruciform specimen is built in the software ABAQUS/Explicit, as shown in Fig. 21. The cruciform specimen is meshed with the C3D8R elements, and the mesh size is refined to 0.2 mm for the thickness reduction region. Five layers of elements are applied in the thickness direction. The numerical biaxial tensile tests of five tensile ratios (4 : 4, 4 : 3, 3 : 2, 4 : 2, and 4 : 1) are conducted. The initial crack of the cruciform specimen during experiment was not captured by the DIC device due to the adopted low acquisition frequency, and is therefore illustrated here by the predicted results. In Fig. 22, the predicted initial cracks for four representative tensile ratios are presented, along with the experimentally measured major strain field just before the crack occurs. For the 4 : 4 biaxial tension, the predicted initial cracks occur in the region adjacent to the specimen center along the rolling direction, which meets the observed localized necking regions in the experiment. The numerical reproduction of the off-center necking phenomenon indicates that the biaxial test attachment or specimen manufacturing errors are not the main factors for this phenomenon, since the biaxial tensile ratios and specimen dimensions in the simulation are ideal.

For the other tensile ratios, the predicted major strain fields match to experimental results with good agreement, and the initial cracks occur at the specimen center. The predicted strain paths and forming limit points are shown in Fig. 23. The forming limit strains are determined in the same method as adopted in the experimental procedure. The predicted FLC is in good agreement with the experimental result in the first quadrant, while the estimate of formability in the second quadrant is slightly higher. The results suggest that the numerical biaxial tensile test is an effective alternative to FLC prediction, and the GTN damage model coupled with Yld2000-3d yield criterion provides good predictability for the formability of DP590 sheets.

6. Conclusions

In this work, a cost-effective mechanical attachment and heating device are developed to provide a solution for in-plane thermal biaxial testing at different tensile ratios. The FLCs of DP590 sheets at ambient and elevated temperatures are characterized by biaxial tensile tests, and the performance of the mechanical attachment is verified. The main findings are summarized as follows.

(1) The novel mechanical attachment exhibits good rigidity and stability, meeting the requirements for biaxial testing of DP590 high-strength alloy materials. By replacing the trapezoidal blocks with different inclination angles, the attachment allows for biaxial testing at six different tensile ratios. The heating device employs a combination of induction heating technology and conduction heating method, enabling a uniform and symmetrical temperature distribution in the main deformation zone of the cruciform specimen.
(2) The thermal biaxial tensile tests reveal a non-monotonic effect of temperature on formability of DP590 sheets. At 300 °C, the FLC of DP590 is lower than that at ambient temperature due to the DSA effects. While at 400 °C and 500 °C, the formability shows significant improvement.
(3) Due to the non-linear strain path effects, the FLC obtained from the Nakazima test exhibits a shift toward positive values of minor strain compared to the FLC obtained from biaxial tensile tests. Notably, the forming limits determined by biaxial tensile tests under equi-biaxial tension is lower than that obtained from the Nakazima test. This discrepancy is attributed to the initial localized necking occurring in an off-center area of the cruciform specimen.
(4) FE simulations, based on the calibrated Yld2000-3d yield criterion and the GTN model, can correctly predict localized necking and fracture for DP590 sheets under biaxial tensions. The predicted FLC agrees well with experimental results.

Declaration of competing interest

The authors declare that they have no known competing financial interests or personal relationships that could have appeared to influence the work reported in this paper.

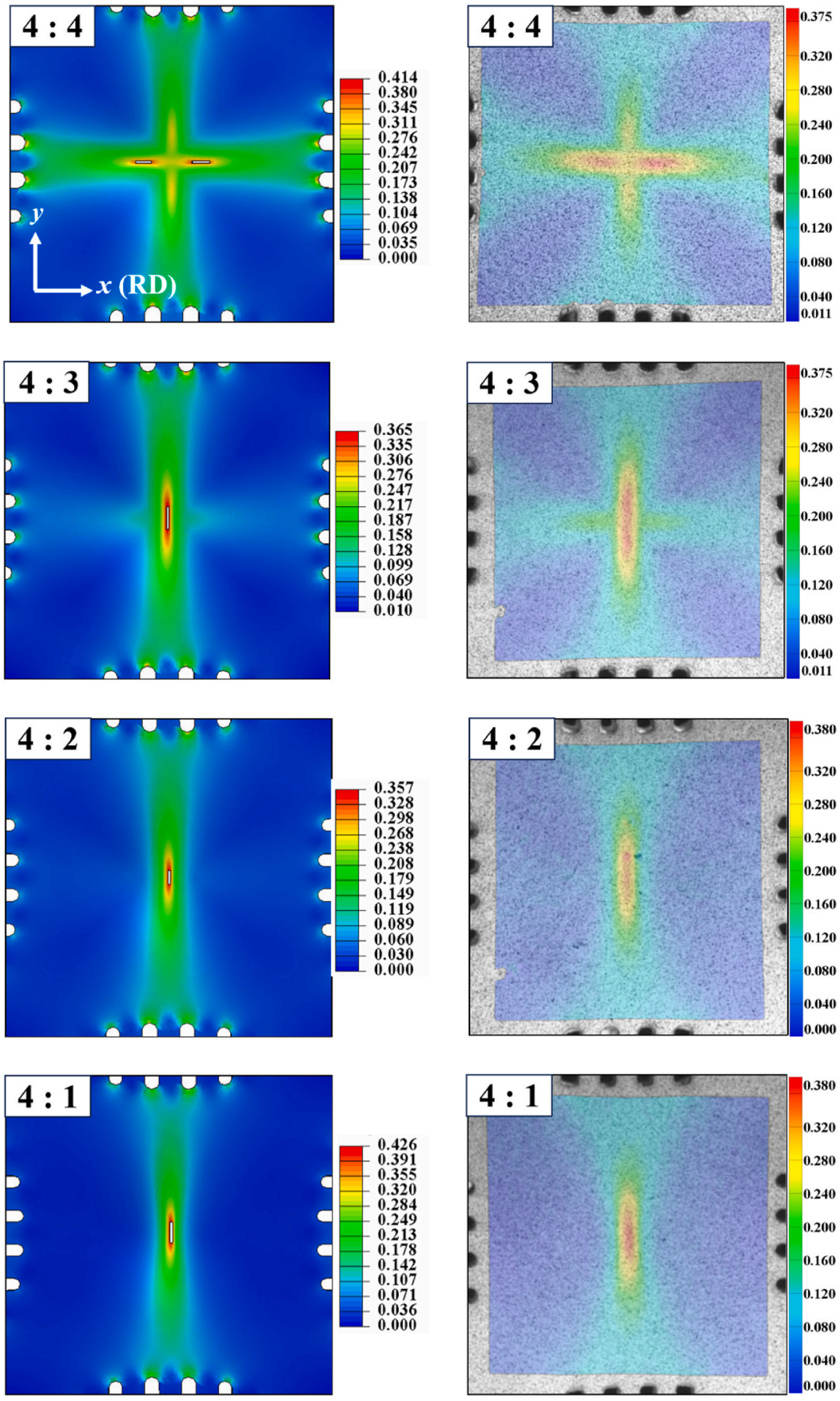

Fig. 22. Predicted major strain fields with initial cracks (on the left) and experimentally measured major strain fields (on the right) of the specimen ROI for four representative tensile ratios. The experimental results are acquired just before fracture occurs.

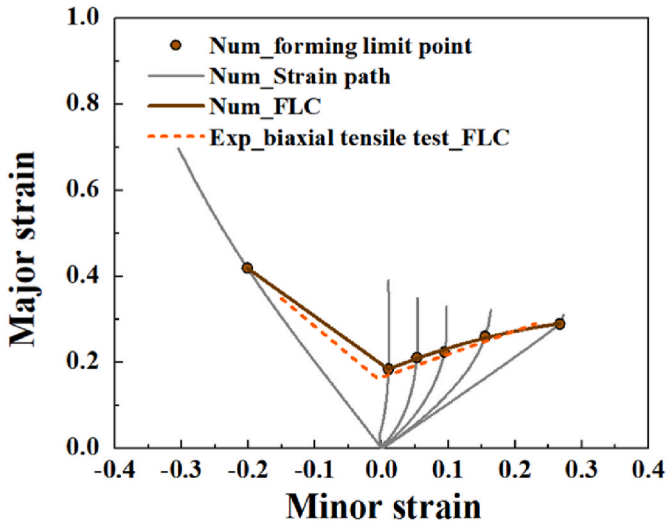

Fig. 23. Predicted FLC using the numerical biaxial tensile tests and the anisotropy GTN model, and compared with the experimentally determined FLC.

Acknowledgments

The authors would like to acknowledge the financial support from National Natural Science Foundation of China (Grant No. 52175339) and Key Research and development program of Shandong province (Grant No. 2021CXGC010304). Z. WANG acknowledges the China Scholarship Council (CSC) for his Ph.D. financial support.

Appendix A. Yld2000-3d yield criterion

The 3D extension of the Yld2000-2d yield criterion [49] proposed by Dunand et al. [41] is defined as :

$$\overline{\sigma}=\frac{1}{2^{1/a}}[\varphi^{'}(\boldsymbol{s}^{'})+\varphi^{''}(\boldsymbol{s}^{''})]^{\frac{1}{a}} \tag{A.1}$$

$$\boldsymbol{s}^{'}=\boldsymbol{L}^{'}\boldsymbol{\sigma},\boldsymbol{s}^{''}=\boldsymbol{L}^{''}\boldsymbol{\sigma} \tag{A.2}$$

The coefficients of $\boldsymbol{L}^{'}$ and $\boldsymbol{L}^{''}$ for linear transformations are expresses as follows:

$$\boldsymbol{L}^{'}=\frac{1}{3}\begin{bmatrix}2\alpha_1 & -\alpha_1 & -\alpha_1 & 0 & 0 & 0\\ -\alpha_2 & 2\alpha_2 & -\alpha_2 & 0 & 0 & 0\\ 0 & 0 & 0 & 3\alpha_7 & 0 & 0\\ 0 & 0 & 0 & 0 & 3\alpha_9 & 0\\ 0 & 0 & 0 & 0 & 0 & 3\alpha_{10}\end{bmatrix} \tag{A.3}$$

$$\boldsymbol{L}^{''}=\frac{1}{9}\begin{bmatrix}-2\alpha_3+2\alpha_4+8\alpha_5-2\alpha_6 & -4\alpha_4+4\alpha_6+\alpha_3-4\alpha_5 & \alpha_3+2\alpha_4-4\alpha_5-2\alpha_6 & 0 & 0 & 0\\ 4\alpha_3-4\alpha_4-4\alpha_5+\alpha_6 & -2\alpha_3+8\alpha_4+2\alpha_5-2\alpha_6 & -2\alpha_3-4\alpha_4+2\alpha_5+\alpha_6 & 0 & 0 & 0\\ 0 & 0 & 0 & 9\alpha_8 & 0 & 0\\ 0 & 0 & 0 & 0 & 9\alpha_{11} & 0\\ 0 & 0 & 0 & 0 & 0 & 9\alpha_{12}\end{bmatrix} \tag{A.4}$$

where α_k (for k from 1 to 12) are material parameters. α_9, …, α_{12} are associated with out-plane shear stresses.

$$\varphi^{'}(\boldsymbol{s}^{'})=\left[\left(s^{'}_{xx}-s^{'}_{yy}\right)^2+4\left(s^{'2}_{xy}+s^{'2}_{xz}+s^{'2}_{yz}\right)\right]^{\frac{a}{2}} \tag{A.5}$$

$$\begin{aligned}\varphi^{''}(\boldsymbol{s}^{''})=&\left[\frac{3}{2}\left(s^{''}_{xx}-s^{''}_{yy}\right)+\frac{1}{2}\sqrt{\left(s^{''}_{xx}-s^{''}_{yy}\right)^2+4\left(s^{''2}_{xy}+s^{''2}_{xz}+s^{''2}_{yz}\right)}\right]^a\\ &+\left[\frac{3}{2}\left(s^{''}_{xx}-s^{''}_{yy}\right)-\frac{1}{2}\sqrt{\left(s^{''}_{xx}-s^{''}_{yy}\right)^2+4\left(s^{''2}_{xy}+s^{''2}_{xz}+s^{''2}_{yz}\right)}\right]^a\end{aligned} \tag{A.6}$$

Appendix B. GTN plasticity model

The GTN plasticity model [48,50,51] is defined as:

$$\Phi = \left(\frac{\bar{\sigma}}{\sigma_y}\right)^2 + 2q_1 f^* \cosh\left(\frac{3q_2\sigma_m}{2\sigma_y}\right) - \left(1 + q_3 f^{*2}\right) = 0 \tag{B.1}$$

where $\bar{\sigma}$ is the equivalent stress, which is calculated using the Yld2000-3d yield criterion in this work. σ_y is the yield stress. q_1, q_2, q_3 are material parameters. f^* is the equivalent void volume fraction.

$$f^* = \begin{cases} f & f \le f_C \\ f_c + \dfrac{1/q_1 - f_C}{f_F - f_C}(f - f_C) & f > f_C \end{cases} \tag{B.2}$$

$$df = (1-f)\boldsymbol{d\varepsilon}^p : \boldsymbol{I} + A_N \cdot d\bar{\varepsilon}^p + k_w f \frac{w[\mathrm{dev}(\boldsymbol{\sigma})]}{\bar{\sigma}} \mathrm{dev}(\boldsymbol{\sigma}) : \boldsymbol{d\varepsilon}^p \tag{B.3}$$

$$A_N = \frac{f_N}{s_N\sqrt{2\pi}} \exp\left(-\frac{1}{2}\left(\frac{\bar{\varepsilon}^p - \varepsilon_N}{s_N}\right)\right) \tag{B.4}$$

where f_N, f_C, f_F, ε_N, s_N, k_w are parameters associated with the evolution of void volume fraction. The third term in Eq. (B.3) was proposed by Nahshon and Hutchinson [40], which considers the dependence of void growth on the third invariant of the deviatoric stress tensor dev($\boldsymbol{\sigma}$). $w[dev(\boldsymbol{\sigma})]$ is defined as:

$$w[\mathrm{dev}(\boldsymbol{\sigma})] = 1 - \left(\frac{27J_3}{2\bar{\sigma}^3}\right)^2 \tag{B.5}$$

where J_3 is the third invariant of the deviatoric stress.

References

[1] Ermolaeva NS, Castro MBG, Kandachar PV. Materials selection for an automotive structure by integrating structural optimization with environmental impact assessment. Mater Des 2004;25(8):689–98. https://doi.org/10.1016/j.matdes.2004.02.021.

[2] Zhang W, Xu J. Advanced lightweight materials for automobiles: a review. Mater Des 2022;221:110994. https://doi.org/10.1016/j.matdes.2022.110994.

[3] Kleiner M, Chatti S, Klaus A. Metal forming techniques for lightweight construction. J Mater Process Technol 2006;177(1–3):2–7. https://doi.org/10.1016/j.jmatprotec.2006.04.085.

[4] Shao Z, Li N, Lin J, Dean T. Formability evaluation for sheet metals under hot stamping conditions by a novel biaxial testing system and a new materials model. Int J Mech Sci 2017;120:149–58. https://doi.org/10.1016/j.ijmecsci.2016.11.022.

[5] Fakir OE, Wang L, Balint D, Dear JP, Lin J, Dean TA. Numerical study of the solution heat treatment, forming, and in-die quenching (HFQ) process on AA5754. Int J Mach Tool Manufact 2014;87:39–48. https://doi.org/10.1016/j.ijmachtools.2014.07.008.

[6] Zhang H, Lin GY, Peng DS, Yang LB, Lin QQ. Dynamic and static softening behaviors of aluminum alloys during multistage hot deformation. J Mater Process Technol 2004;148(2):245–9. https://doi.org/10.1016/j.jmatprotec.2003.12.020.

[7] Huang K, Loge RE. A review of dynamic recrystallization phenomena in metallic materials. Mater Des 2016;111:548–74. https://doi.org/10.1016/j.matdes.2016.09.012.

[8] Li YL, Kohar CP, Muhammad W, Inal K. Precipitation kinetics and crystal plasticity modeling of artificially aged AA6061. Int J Plast 2022;152:103241. https://doi.org/10.1016/j.ijplas.2022.103241.

[9] Zheng K, Politis DJ, Wang L, Lin J. A review on forming techniques for manufacturing lightweight complex-shaped aluminium panel components. Int J Lightweight Mater Manuf 2018;1(2):55–80. https://doi.org/10.1016/j.ijlmm.2018.03.006.

[10] Hannon A, Tiernan P. A review of planar biaxial tensile test systems for sheet metal. J Mater Process Technol 2008;198(1–3):1–13. https://doi.org/10.1016/j.jmatprotec.2007.10.015.

[11] Liu W, Guines D, Leotoing L, Ragneau E. Identification of strain rate-dependent mechanical behaviour of DP600 under in-plane biaxial loadings. Mater Sci Eng, A 2016;676:366–76. https://doi.org/10.1016/j.msea.2016.08.125.

[12] Zhang S, Leotoing L, Guines D, Thuillier S, Zang SL. Calibration of anisotropic yield criterion with conventional tests or biaxial test. Int J Mech Sci 2014;85:142–51. https://doi.org/10.1016/j.ijmecsci.2014.05.020.

[13] Wang Z, Guines D, Chu X, Leotoing L. Prediction and characterization of forming limits at necking from shear to equi-biaxial loading using the biaxial tensile testing method: feasibility study and application to AA6061-T4. Mech Mater 2023;179:104598. https://doi.org/10.1016/j.mechmat.2023.104598.

[14] Wang Z, Guines D, Chu X, Leotoing L. Characterization of forming limits at fracture from shear to plane strain with a dedicated cruciform specimen. Int J Material Form 2022;15:7. https://doi.org/10.1007/s12289-022-01658-8.

[15] Leotoing L, Guines D, Zidane I, Ragneau E. Cruciform shape benefits for experimental and numerical evaluation of sheet metal formability. J Mater Process Technol 2013;213(6):856–63. https://doi.org/10.1016/j.jmatprotec.2012.12.013.

[16] Kuwabara T, Ikeda S, Kuroda K. Measurement and analysis of differential work hardening in cold-rolled steel sheet under biaxial tension. J Mater Process Technol 1998;80–81:517–23. https://doi.org/10.1016/S0924-0136(98)00155-1.

[17] Leotoing L, Guines D. Investigations of the effect of strain path changes on forming limit curves using an in-plane biaxial tensile test. Int J Mech Sci 2015;99:21–8. https://doi.org/10.1016/j.ijmecsci.2015.05.007.

[18] Chen J, Zhang J, Zhao H. Development and experimental verification of a high-temperature and in-plane biaxial testing apparatus. Machines 2022;10:1054. https://doi.org/10.3390/machines10111054.

[19] Tierriault P, Settouane K, Brailovski V. Biaxial testing at different temperatures of cruciform Ti-Ni samples. In: Proceedings of the International Conference on Shape Memory and Superplastic Technologies; 2003. p. 247–57. https://doi.org/10.1361/cp2003smst247.

[20] Barroso A, Correa E, Freire J, Paris F. A device for biaxial testing in uniaxial machines. design, manufacturing and experimental results using cruciform specimens of composite materials. Exp Mech 2018;58:49–53. https://doi.org/10.1007/s11340-017-0327-6.

[21] Bhatnagar N, Bhardwaj R, Selvakumar P, Brieu M. Development of a biaxial tensile test fixture for reinforced thermoplastic composites. Polym Test 2007;26:154–61. https://doi.org/10.1016/j.polymertesting.2006.09.007.

[22] Merklein M, Biasutti M. Development of a biaxial tensile machine for characterization of sheet metals. J Mater Process Technol 2013;213:939–46. https://doi.org/10.1016/j.jmatprotec.2012.12.005.

[23] Shao Z, Li N, Lin J, Dean TA. Development of a new biaxial testing system for generating forming limit diagrams for sheet metals under hot stamping conditions. Exp Mech 2016;56:1489–500. https://doi.org/10.1007/s11340-016-0183-9.

[24] Abedrabbo N, Pourboghrat F, Carsley J. Forming of aluminum alloys at elevated temperatures - Part 1: material characterization. Int J Plast 2006;22(2):314–41. https://doi.org/10.1016/j.ijplas.2005.03.005.

[25] Khan AS, Suh YS, Kazmi R. Quasi-static and dynamic loading responses and constitutive modeling of titanium alloy. Int J Plast 2004;20:2233–48. https://doi.org/10.1016/j.ijplas.2003.06.005.

[26] Li Z, Zhou G, Li D, Jain MK, Peng Y, Wu P. Forming limits of magnesium alloy AZ31B sheet at elevated temperatures. Int J Plast 2020;135:102822. https://doi.org/10.1016/j.ijplas.2020.102822.

[27] Zhao J, Jiang Z. Thermomechanical processing of advanced high strength steels. Prog Mater Sci 2018;94:174–242. https://doi.org/10.1016/j.pmatsci.2018.01.006.

[28] Liang J, Guines D, Leotoing L. Effect of temperature and strain rate on the plastic anisotropic behavior characterized by a single biaxial tensile test. Procedia Manuf 2020;47:1532–9. https://doi.org/10.1016/j.promfg.2020.04.346.

[29] Zhang R, Shi Z, Yardley VA, Lin J. Experimental studies of necking and fracture limits of boron steel sheet under hot stamping conditions. J Mater Process Technol 2022;302:117481. https://doi.org/10.1016/j.jmatprotec.2021.117481.

[30] Xiao R, Li XX, Lang LH, Chen YK, Yang YF. Biaxial tensile testing of cruciform slim superalloy at elevated temperatures. Mater Des 2016;94:286–94. https://doi.org/10.1016/j.matdes.2016.01.045.

[31] Jiang H, Nguyen TH, Prud'homme M. Optimal control of induction heating for semi-solid aluminum alloy forming. J Mater Process Technol 2007;189:182–91. https://doi.org/10.1016/j.jmatprotec.2007.01.020.

[32] Song X, Leotoing L, Guines D, Ragneau E. Characterization of forming limits at fracture with an optimized cruciform specimen: application to DP600 steel sheets. Int J Mech Sci 2017;126:35–43. https://doi.org/10.1016/j.ijmecsci.2017.03.023.

[33] Li X, Roth CC, Bonatti C, Mohr D. Counterexample-trained neural network model of rate and temperature dependent hardening with dynamic strain aging. Int J Plast 2022;151:103218. https://doi.org/10.1016/j.ijplas.2022.103218.
[34] Simsir C, Cetin B, Efe M, Davut K, Bayramin B. A material perspective on consequence of deformation heating during stamping of DP steels. J Phys: Conf Ser 2017;896:012059. https://doi.org/10.1088/1742-6596/896/1/012059.
[35] Shen F, Munstermann S, Lian J. An evolving plasticity model considering anisotropy, thermal softening and dynamic strain aging. Int J Plast 2020;132: 102747. https://doi.org/10.1016/j.ijplas.2020.102747.
[36] Bayramin B, Simsir C, Efe M. Dynamic strain aging in DP steels at forming relevant strain rates and temperatures. Mater Sci Eng 2017;704:164–72. https://doi.org/10.1016/j.msea.2017.08.006.
[37] Zhang R, Shi Z, Shao Z, Yardley VA, Lin J, Dean TA. Biaxial test method for determination of FLCs and FFLCs for sheet metals: validation against standard Nakajima method. Int J Mech Sci 2021;209:106694. https://doi.org/10.1016/j.ijmecsci.2021.106694.
[38] Soyarslan C, Malekipour Gharbi M, Tekkaya AE. A combined experimental-numerical investigation of ductile fracture in bending of a class of ferritic-martensitic steel. Int J Solid Struct 2012;49:1608–26. https://doi.org/10.1016/j.ijsolstr.2012.03.009.
[39] Xue L. Localization conditions and diffused necking for damage plastic solids. Eng Fract Mech 2010;77:1275–97. https://doi.org/10.1016/j.engfracmech.2009.12.008.
[40] Nahshon K, Hutchinson JW. Modification of the Gurson model to shear failure. Eur J Mech Solid 2008;27:1–17. https://doi.org/10.1016/j.euromechsol.2007.08.002.
[41] Dunand M, Maertens AP, Luo M, Mohr D. Experiments and modeling of anisotropic aluminum extrusions under multi-axial loading - Part I: plasticity. Int J Plast 2012; 36:34–49. https://doi.org/10.1016/j.ijplas.2012.03.003.
[42] Kavanagh KT, Clough RW. Finite element applications in the characterization of elastic solids. Int J Solid Struct 1971;7(1):11–23. https://doi.org/10.1016/0020-7683(71)90015-1.
[43] Avril S, Bonnet M, Bretelle AS, Grediac M, Hild F, Ienny P, et al. Overview of identification methods of mechanical parameters based on full-field measurements. Exp Mech 2008;48:381–402. https://doi.org/10.1007/s11340-008-9148-y.
[44] Martins JMP, Andrade-Campos A, Thuillier S. Calibration of anisotropic plasticity models using a biaxial test and the virtual fields method. Int J Solid Struct 2019; 172–173:21–37. https://doi.org/10.1016/j.ijsolstr.2019.05.019.
[45] Martins JMP, Andrade-Campos A, Thuillier S. Comparison of inverse identification strategies for constitutive mechanical models using full-field measurements. Int J Mech Sci 2018;145:330–45. https://doi.org/10.1016/j.ijmecsci.2018.07.013.
[46] Luo M, Dunand M, Mohr D. Experiments and modeling of anisotropic aluminum extrusions under multi-axial loading - Part II: ductile fracture. Int J Plast 2012; 32–33:36–58. https://doi.org/10.1016/j.ijplas.2011.11.001.
[47] Yoon JW, Barlat F, Dick RE, Chung K, Kang TJ. Plane stress yield function for aluminum alloy sheets - part II: FE formulation and its implementation. Int J Plast 2004;20:495–522. https://doi.org/10.1016/S0749-6419(03)00099-8.
[48] Tvergaard V, Needleman A. Analysis of the cup-cone fracture in a round tensile bar. Acta Metall 1984;32:157–69.
[49] Barlat F, Brem JC, Yoon JW, Chung K, Dick RE, Lege DJ, et al. Plane stress yield function for aluminum alloy sheets - Part I: theory. Int J Plast 2003;19(9): 1297–319. https://doi.org/10.1016/S0749-6419(02)00019-0.
[50] Gurson AL. Continuum theory of ductile rupture by void nucleation and growth Part I - yield criteria and flow rules for porous ductile media. J Eng Mater Technol 1977;99:2–15. https://doi.org/10.1115/1.3443401.
[51] Tvergaard V. Influence of voids on shear band instabilities under plane strain conditions. Int J Fract 1981;17:389–407. https://doi.org/10.1007/BF00036191.